Catalysis Today 166 (2011) 152–158

Contents lists available at ScienceDirect

Catalysis Today

journal homepage: www.elsevier.com/locate/cattod

TiO_2 doped with Sm^{3+} by sol–gel: Synthesis, characterization and photocatalytic activity of diuron under solar light

D. de la Cruz [a,b], J.C. Arévalo [b,c], G. Torres [b,*], R.G. Bautista Margulis [c], C. Ornelas [a], A. Aguilar-Elguézabal [a]

[a] Centro de Investigación en Materiales Avanzados, CIMAV, Av. Miguel de Cervantes 120, Complejo Industrial, Chihuahua, Chih. C.P. 31109, Mexico
[b] Universidad Juárez Autónoma de Tabasco, Laboratorio de Catálisis Heterogénea, DACB, Km. 1 Carr. Cunduacán-Jalpa de Méndez, C.P. 86690, A.P. 24, Cunduacán, Tabasco, Mexico
[c] Universidad Juárez Autónoma de Tabasco, DACBiol, Km. 0.5 Carretera Villahermosa-Cárdenas, entronque a bosques de saloya, C.P. 86150, Villahermosa, Tabasco, Mexico

ARTICLE INFO

Article history:
Available online 14 October 2010

Keywords:
TiO_2 doped Sm^{3+}
Sol–gel
Synthesis and characterization
Photocatalytic diuron
Solar light

ABSTRACT

A simple method to synthesize highly dispersed Sm^{3+} on TiO_2 by sol–gel which induced significant changes in the photocatalytic properties, Eg values, specific surface areas, and crystal size of pure TiO_2, is reported. As is well known, thermal treatment of anatase TiO_2 at 600 °C leads to the transformation to rutile phase, however for Sm^{3+} doped photocatalyst here reported, a significant amount of anatase phase remained even after thermal treatment at 800 °C, showing an interesting photocatalytic activity under sunlight degradation of diuron. TiO_2 doped with 0.3 wt% Sm^{3+} and calcined at 500 °C showed the best performance for the photocatalytic degradation of diuron herbicide.

1. Introduction

For photocatalytic applications, TiO_2 presents a low quantum yield due to the fast recombination between photogenerated conduction band electrons (e^-) and holes (h^+) [1]. There have been attempts to improve the efficiency of charge separation in order to reduce recombination events, due to the fact that these species must be available in the reaction medium to promote the degradation of organic molecules around titania surroundings. One way to decrease electron-hole recombination has been attempted through the control of periodic illumination (avoiding excessive concentration of e^-, h^+ pairs and promoting thus the oxidation/reduction reaction of chemical species before the introduction of more photons into the system) [2] and the application of an electrical bias [3]. In order to improve photocatalytic TiO_2 performance, titania has been doped with different metals and oxides as La^{3+}, Ce^{3+}, Er^{3+}, Pr^{3+}, Gd^{3+}, Nd^{3+}, Sm^{3+}, Cd, and Eu^{3+}, which can efficiently extend the light absorption properties to the visible region and the absorption coefficient *K* augment strongly increasing the photocatalytic powder of TiO_2 [4–7]. Diuron is a common herbicide that is identified as an important pollutant of soil and water. The environment favors diuron degradation due to physical–chemical characteristics of soil, as well as free radicals, and bacteria present in soil. Nevertheless, this is a very slow process and is highly dependent of the climatic and geographic conditions [8]. For these reasons, research has been carried out to find new ways to eliminate diuron in a quick and safe way [9–14]. In this work TiO_2 doped with Sm^{3+} at 0.3 and 0.5 wt% was prepared by sol–gel method and calcined at 500 and 800 °C. These materials were applied on the photocatalytic oxidation of diuron sunlight radiation.

2. Experimental

2.1. Preparation of TiO_2

TiO_2 was obtained by the sol–gel method using titanium n-butoxide as the precursor from Aldrich (97% of purity). A mixture of butanol–water was stirred and kept in reflux at 70 °C. Titanium n-butoxide was added drop by drop for 3 h to this solution until a gel was formed, then NH_4OH was added to the mixture until a pH of 7 was reached. This mixture was stirred with reflux at 70 °C during 24 h. After this time, the gel was dried in a rotary evaporator at 80 °C under vacuum. Afterwards, the powder was dried in a oven at 120 °C during 12 h. The samples were calcined at 500 °C and 800 °C during 4 h at a heating rate of 2 °C/min.

2.2. Preparation of TiO_2 doped with Sm^{3+}

The materials doped with Sm^{3+} were obtained by using samarium nitrate precursor salt. Samarium aqueous solutions were obtained by the stoichiometric addition of precursor to obtain 0.3 wt% or 0.5 wt% of Sm^{3+} in all titania doped samples. For doped photocatalysts the same methodology used to obtain the TiO_2 without doping was followed and the dopant was added to a

* Corresponding author. Tel.: +52 914 336 0300; fax: +52 914 336 0928.
E-mail addresses: gilberto.torres@dacb.ujat.mx, torremensajes@gmail.com (G. Torres).

0920-5861/$ – see front matter © 2010 Elsevier B.V. All rights reserved.
doi:10.1016/j.cattod.2010.08.023

butanol–butoxide mixture before adding it to the aqueous solution of butanol–water.

2.3. Characterization techniques

2.3.1. BET surface specific area

Micromeritics ASAP 2020 equipment was used to obtain the specific surface area and pore diameter distribution. Results were calculated from nitrogen adsorption isotherms. Before measuring, the samples were outgassed at 350 °C during 2 h.

2.3.2. X-ray diffraction

Diffractograms were obtained by a SIEMENS-D500 diffractometer equipped with a Cu anode with Kα radiation and a graphite monochromator was used to obtain X-ray diffraction (XRD) spectra. The samples were scanned in the range of 2θ from 20° to 70° with a 0.02° step at a rate of 1 s/point. Crystalline structures were identified through the use of the Joint Committee on Powder Diffraction Standards (JCPDS) library.

2.3.3. FT-Raman

Spectra were obtained by a PerkinElmer Spectrum GX NIR-FT Raman spectrometer equipped with a microscope and CCD detector. Spectra were taken at room temperature and using a 5145 Å line and argon ion laser (model spectra physics 2020) excited with of 50 mV of energy.

2.3.4. Ultraviolet visible spectrometry

A Varian Cary-III Ultraviolet visible (UV–vis) spectrophotometer with diffuse reflectance and fitted with an integrated sphere was used to obtain the absorption spectra of photocatalysts. The transmission mode was used to follow the concentration changes of diuron in the aqueous solutions during photocatalytic activity tests.

2.3.5. STEM-EELS and STEM-EDS

STEM-ELLS and STEM-EDS analyses were carried out using a field emission electron microscope equipped with spherical aberration corrector, model JEOLJEM2200FS+CS.

2.3.6. Photocatalytic activity of TiO_2 materials

The tests were carried out into a 100 mL quartz vessel photoreactor (see Fig. 1), which include a cooling system inside in order to avoid the evaporation of solution preserving the temperature of the reaction constant. The reactor has an inlet to fed oxygen, the inlet for catalyst and prepared solution (contaminated water) and one valve to take samples periodically during the reactions. A magnetic stirrer is placed inside of the solution to homogenize the solution with the catalyst. 70 mL of aqueous solution of diuron with a concentration of 40 ppm was prepared and placed into the reactor, then depending on test, 0.5 g of doped or undoped TiO_2 were loaded, and stirring was started. In each activity test a fresh photocatalyst was used. Finally, the oxygen was fed and regulated to a 60 cm^3/min in order to supply the required quantity of oxygen to accomplish the photocatalytic reactions. Sunlight was used as radiation source; the reactor was placed on the roof of the laboratory building where solar radiation is intense between 11 and 15 h because at these hours the measured radiation reaches the maximum value (2.7–3.0 mW/cm^2), then the reactions were carried out at these hours. The radiation values were measured using a NR-LITE Net Radiometer with a measurement range of ±2000 W m^{-2} and a sensitivity of 10 μV W^{-1} m^2. The radiation was measured simultaneously to reaction tests. During the reaction, aliquots were taken out each 30 min and then were analyzed by the above mentioned spectrometer.

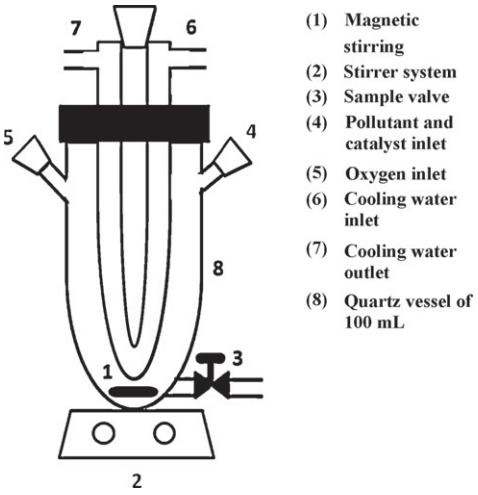

Fig. 1. Photoreactor employed under sunlight irradiation constructed in quartz.

3. Results and discussion

3.1. Material characterization

3.1.1. Textural properties

Doped TiO_2 was synthesized under careful control of conditions in order to obtain materials with appropriate textural characteristics for photocatalytic solar degradation of organic compounds. As can be seen from Table 1, when Sm is introduced into TiO_2 and calcined to 500 °C, specific surface area increases, being the sample doped with 0.5 wt% which exhibited the highest increase (1.33% with respect to pure TiO_2). According to the element distribution mapping obtained by STEM-EDS (see Fig. 2), high dispersion of the dopant samarium was reached on the TiO_2, this results agree with the reported by other authors which use a low percentage of lanthanum as a dopant [15].

Doped photocatalysts calcined at 500 °C presented practically equivalent pore size diameters to that of pure TiO_2. Pore diameter for calcined solids at 800 °C increased for all samples. Most of the materials presented unimodal distributions, only the Sm^{3+}/TiO_2 with 0.5 wt% and calcined at 800 °C showed bimodal distribution and their pore diameter exceeded 100 nm; it was established that grain coalescence and phase transition in TiO_2 are affected by

Table 1
Results of specific surface area, phase (%) calculated by XRD patterns of the photocatalysts prepared by sol–gel method.

Photocatalyst	T_c (°C)	S_{BET} (m^2/g)	P_D (nm)	Type of pore	Phase %
TiO_2	500	78.7	7.9	Unimodal	A*
Sm/TiO_2 0.3%	500	95.7	8.4	Unimodal	A*
Sm/TiO_2 0.5%	500	95.9	8.4	Unimodal	A*
TiO_2	800	16.7	32.0	Unimodal	R*
Sm/TiO_2 0.3%	800	24.7	30.7	Unimodal	A*–R* (28–72)
Sm/TiO_2 0.5%	800	16.1	111.0	Bimodal	A*–R* (31–69)

*A: anatase; *R: rutile.

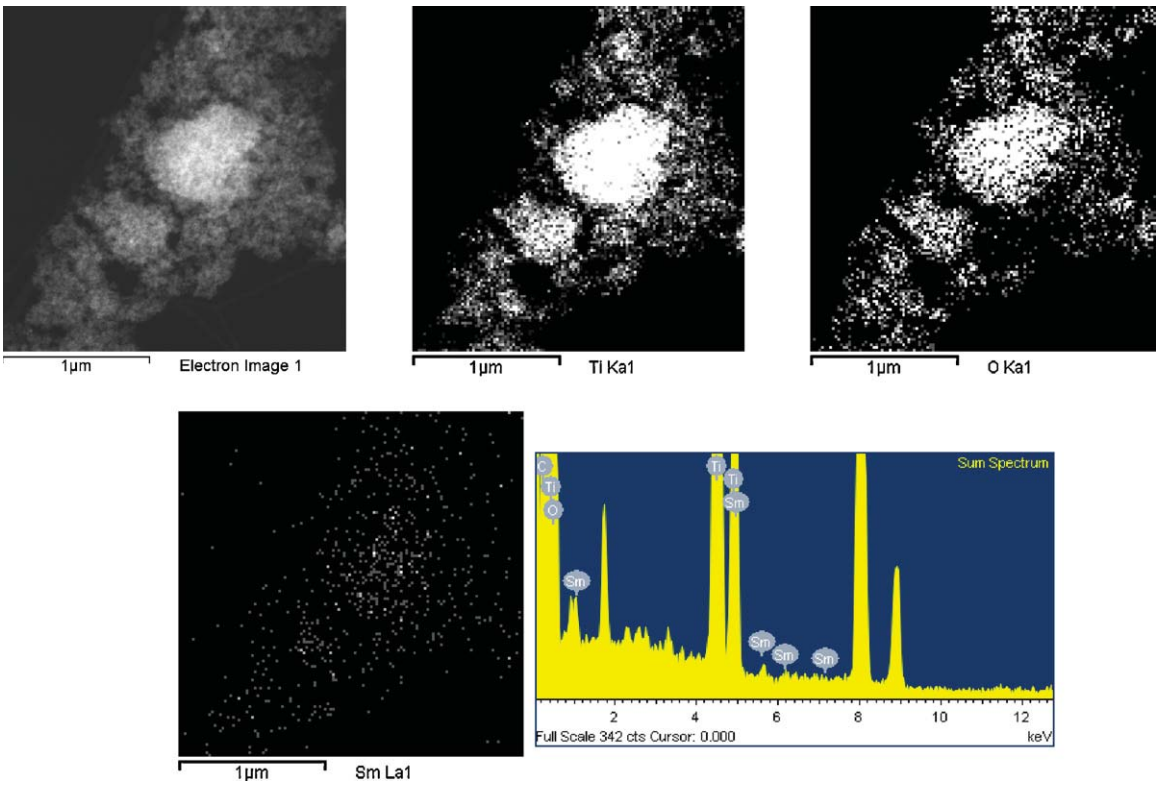

Fig. 2. STEM-EDS spectra of TiO_2 doped with Sm^{3+} (0.5 wt%) calcinated to 500 °C.

the presence of dopants. Anatase can indeed be conceived as an arrangement of parallel Ti–O octahedral while for rutile some of the octahedral are rotated by 90° [16–18]. Thereby, conversion from anatase to rutile can be regarded in terms of rearrangement of octahedral orientation [19] with a symmetry change from the $I4_1/amd$ to $P4_2/mnm$ space group. A study with Ta and Nb as dopant [20] showed that stabilization of nanosized structure of titania with these dopants was due to substitution of Ti^{4+} by rare earth element in the TiO_2 lattice. The presence of the dopant in a nanostructure can affect the rate of grain growth and the density of rutile nucleation sites via two basic mechanisms: (I) segregation at the grain boundary of a phase lowering the surface energy of the grains or (II) by the occupation of bulk lattice sites in such a way to hinder the ionic mobility. It has been reported in the literature that nucleation of rutile occurs at either grain's surface, at the boundary among particles, or in the bulk [21]. In particular, boundary nucleation results in significantly larger rutile particles, because one or more anatase grains are merged into a single rutile particle. Rutile nucleation within anatase bulk grains requires high activation energy and therefore would occur at higher temperature. These mechanisms are present during calcining treatment of Sm^{3+}/TiO_2.

3.1.2. X-ray diffraction

Fig. 3 shows the diffractograms for TiO_2 calcined at 500 (a) and 800 °C (b). In general, only two phases were detected: anatase and rutile. The diffractogram of the TiO_2 which was calcined at 500 °C corresponds to the anatase phase (see Fig. 3a). For the sample calcined at 800 °C, well-defined signals were observed, which consisted of intense and sharp peaks due to the high crystallinity of the rutile (see Fig. 3b). By using the Scherrer equation ($dP = k\lambda/\beta\cos\theta$), it was determined that the crystal size for the TiO_2 calcined at 500 °C was 8.14 nm and for the photocatalyst calcined at 800 °C elemental crystal size is around 32.7 nm.

The XRD patterns for materials doped with Sm at 0.3 wt% and 0.5 wt% and calcined at 500 °C and 800 °C are shown in Fig. 4. The existence of a mixture of crystalline phases in the TiO_2 was confirmed. In this figure, the peaks corresponding to the anatase and rutile phases appear. As can be seen, despite the treatment at 800 °C, the expected phase transformation of anatase to rutile does not occur, and only a partial change is observed. According to this, the presence of the rare earth has a stabilizer effect on the crystalline structure of titania. Table 1 shows the percentages of crystalline phases present in each of the solids doped with Sm^{3+} at 0.3 wt% and 0.5 wt% and calcined at 800 °C. This estimation was calculated from XRD patterns shown in Fig. 4 using the equation of $\%R = 1/((0.8I_A/I_R) + 1)$. All the materials calcined at 500 °C shown only the signal corresponding to the anatase phase (see Table 1). When the materials were calcined at 800 °C, the TiO_2 without Sm^{3+} doping was transforming entirely to rutile (see Fig. 3 and Table 1), however for the materials doped with Sm^{3+} a mixture of phases

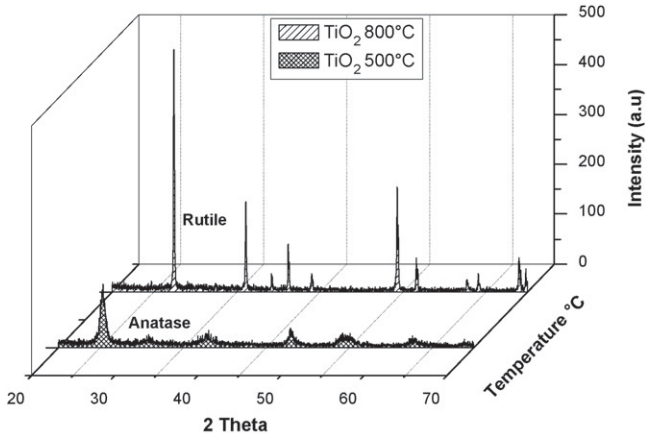

Fig. 3. XRD patterns of (a) TiO_2 calcinated at 500 °C (anatase phase) and (b) TiO_2 calcinated at 800 °C (rutile phase).

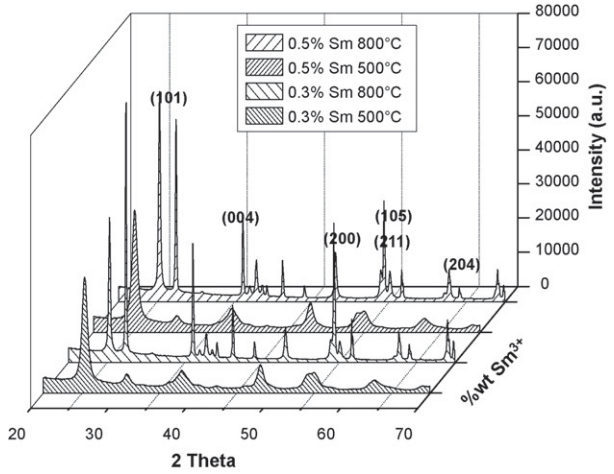

Fig. 4. XRD patterns of TiO_2 doped with 0.3% and 0.5% Sm, calcinated at 500 and 800 °C.

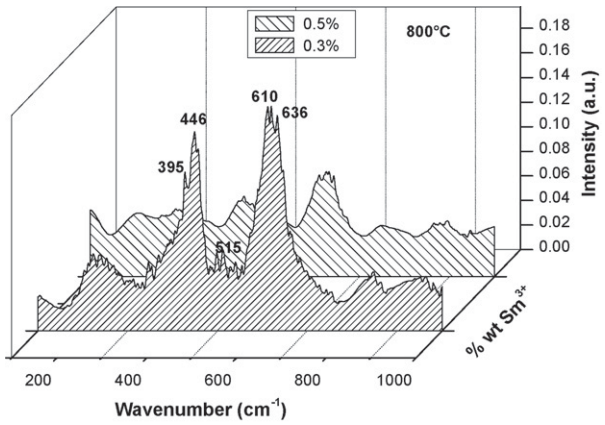

Fig. 6. Raman spectra of TiO_2 doped with Sm^{3+} at 0.3 and 0.5%, calcinated at 800 °C.

was found. For the photocatalyst 0.3 wt% of Sm^{3+}, 28% anatase–72% rutile ratio was calculated and for the photocatalyst 0.5 wt% of Sm^{3+}, calculated ratio of phases was 31% anatase–69% rutile. The ratio of phases of the photocatalyst prepared in this work differs from the commercial Degussa P25 TiO_2 (80% anatase–20% rutile) which is well known for its high photocatalytic activity. It is evident that the dopants provided certain stability and retained the anatase phase since calcination treatments always tended to transform anatase to rutile, and in the synthesized TiO_2 without Sm^{3+}, anatase phase was transformed to rutile at 800 °C as was explained above.

3.1.3. Raman spectroscopy

Raman analysis was carried out in order to identify the crystalline phases in pure TiO_2 and in doped TiO_2 samples and as a complementary technique for the XRD. According to Fig. 5, the characteristic bands which correspond to anatase phases (638 cm^{-1}, 514 cm^{-1}, 398 cm^{-1}) and rutile (608 cm^{-1}, 444 cm^{-1}) [22] were found. At 500 °C only the anatase phase was present with the corresponding peaks of 321 cm^{-1}, 241 cm^{-1} and 198 cm^{-1} attributed to Ti–O–Ti bonds [16]. For the sample calcined at 800 °C only the characteristic bands of the rutile phase (608 cm^{-1}, 444 cm^{-1}) are observed, and a plateau is present at 220 cm^{-1} which is not very steep due to the fact that the unitary cell of the rutile had less Ti–O–Ti bonds in comparison to the anatase phase cell. For this reason the bands at 321 cm^{-1}, 241 cm^{-1}, and 198 cm^{-1} disappear in

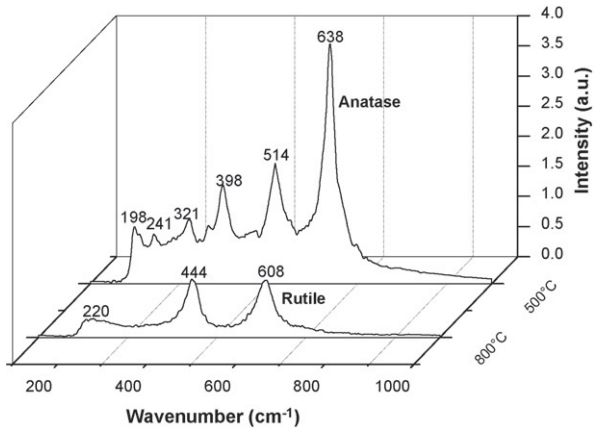

Fig. 5. . Raman spectra of TiO_2 calcinated at 500 °C (anatase) and TiO_2 calcinated at 800 °C (rutile).

the TiO_2 samples calcined at 500 °C. The Raman spectra of solids doped with 0.3 wt% and 0.5 wt% of Sm^{3+} and calcined at 800 °C are shown in Fig. 6. In comparison to the TiO_2 samples without dopant shown in Fig. 5, the 0.3 wt% and 0.5 wt% Sm^{3+} doped samples present characteristic bands of anatase and rutile phases. This is a mixture of both phases that reveals semi-stabilization of the anatase–rutile transition which should be complete as in the case of the TiO_2. The band at 220 cm^{-1} can also be seen and is due to Ti–O–Ti bonds. Lin et al. [23] studied previously the anatase phase transition to rutile; in their results the XRD spectrums showed that the presence of the La_2O_3, Y_2O_3 and CeO_2 at 0.5 wt% stabilized the anatase phase at 650 °C for La, and at 700 °C for Y and Ce. They explained these phenomena by the fact that in the interface, the titanium atoms replace the elements of rare earth in the rare earth oxide surface to form tetragonal sites of the titanium atoms. The interactions between tetrahedron and octahedrons titanium sites restrain the transformation of the anatase phase to the rutile phase during thermal treatments. Another similar explanation was reported by another research group [24]. They explained that in the mixture TiO_2/SiO_2 (30/70 ratio) the anatase phase stabilization occurs by the biphasic surrounding of the SiO_2 in the Ti–O–Si bond. The titanium atoms are substituted into tetrahedral SiO_2 forming Ti tetrahedral sites. The interaction between tetrahedral/octahedral sites of Ti is the responsible of the anatase rutile transformation. The SiO_2 presence in the lattice Ti–O at the interphase with the Ti sites is the responsible of the inhibition of the nucleation phenomena, which is the major phenomenon of anatase–rutile transformation. In Fig. 6, there is an overlapping of the 610 cm^{-1} and 636 cm^{-1} peaks; the first corresponds to the rutile phase and the second to the anatase phase. The same occurs with the peaks at 446 cm^{-1} and 395 cm^{-1} which gives a clear indication of the coexistence of the crystalline phase mixtures (anatase and rutile, exactly as was determined by XRD) which were brought about by the presence of the dopants in the TiO_2 and were well dispersed. This was corroborated by STEM-EDS (see Fig. 2) mapping analysis. The effect of the dopants was to partially stabilize the anatase phase, forming thus materials with different crystalline structures due to the variation of mixtures in accordance to quantity of Sm^{3+} dopant. Calcination at 800 °C should give a complete transition towards the rutile phase [22]. In association to pure TiO_2, the spectra showed a peak at 515 cm^{-1} confirming the presence of the anatase phase. The large presence of the rutile phase indicates a defined crystalline structure. As it can be observed in Fig. 6, the increase on dopant content leads to a decrease of the intensity of signals. This phenomenon is due to the interstitial formation of the Ti–O–M bonds as dopant diffuse to the structure; i.e., in the TiO_2 surface, some TiO_6 cells are able to share an oxygen atom because of the introduction of the dopant metal to form oxides of the dopant metal

Table 2
Results of Sm^{3+} quantities measured by STEM-EDS, band gap calculates by UV–vis DRS spectra and kinetic constant for the photocatalytic diuron destruction.

Photocatalyst	T_c (°C)	Sm^{3+} by STEM-EDS	Eg (eV)	Kinetic constant (min^{-1})
TiO_2	500	–	3.02	0.0041
TiO_2	800	–	2.90	0.0012
Sm/TiO_2	500	0.28	3.10	0.0086
Sm/TiO_2	800	0.31	2.80	0.0074
Sm/TiO_2	500	0.49	3.09	0.0042
Sm/TiO_2	800	0.52	2.80	0.0052

in a tetrahedral form in the vertices of the octahedron and manifest itself through the whole surface in the form of defects. For this reason the intensity of the peaks obtained by Raman spectroscopy decrease for a dopant content increase. This could be explained by the higher content of cells which form the Ti–O–M bond. Furthermore, they do not reflect intense signals from the anatase phase, but a series of peaks and plateaus that are attributed to surface defects.

3.1.4. UV–vis spectroscopy

In Table 2, it can be seen that, in all solids, Eg moved with respect to the theoretical value, resulting in 3.02 eV for TiO_2 and 500 °C (anatase) and 2.9 eV for the TiO_2 at 800 °C (rutile). This caused a shift in absorption towards areas with less energy. Furthermore, it can be observed that most of the solids presentas the raising of radiation absorption in a wavelength equal or higher than 400 nm (see Fig. 7). Typically, titanium dioxide has absorption at 360 nm and as can be seen, TiO_2 without dopant presents absorption from 410 nm. A possible explanation of the displacement of the absorption band can be the insertion of some nitrogen atoms substituting oxygen due to synthesis conditions since NH_4OH was used as hydrolysis catalyst in sol–gel. The displacement of band absorption towards visible radiation by the insertion of nitrogen is well known [25]. The same is true when samples were calcined at 800 °C; there exists a reduction in gap band (or an increase in the length of absorption) due to the modification of the crystalline phase. As can be seen from Fig. 7, Sm^{3+} doped materials also show a displacement on radiation absorption towards the region of the visible light, and the value is near to 400 nm for the two samples calcined at 500 °C. Pure TiO_2 (containing N) presents the absorption at 410 nm, this trend can be attributed to the competition phenomena between Sm^{3+} and N during sol–gel synthesis and probably the amount of N is higher in the TiO_2 without Sm^{3+}. Since all the materials showed radiation absorption within visible region, they can be used for photocatalytic degradation of organic compounds with solar radiation.

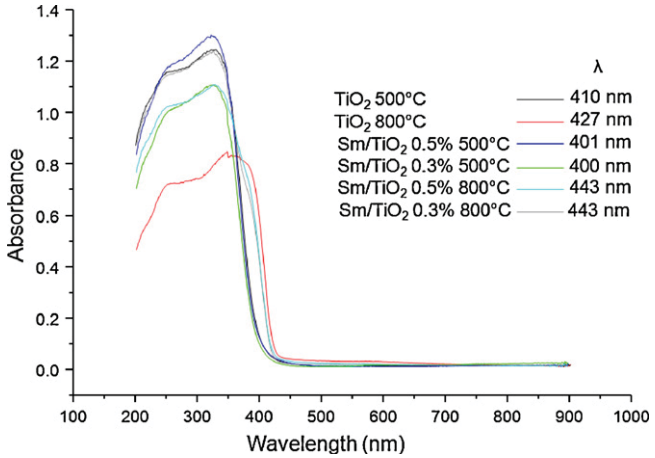

Fig. 7. UV–vis RDS spectra of the photocatalysts.

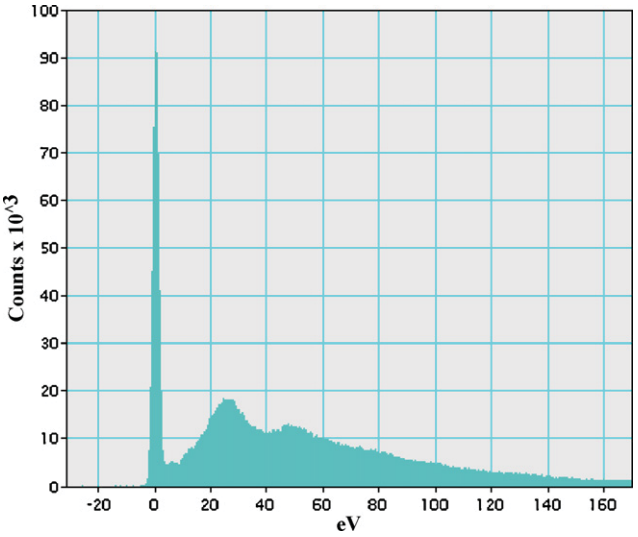

Fig. 8. STEM-EELS spectra of TiO_2 doped with Sm^{3+} (0.5 wt%) calcinated to 500 °C.

3.1.5. STEM-EDS and STEM-EELS analysis

In Fig. 2 the STEM-EDS analysis is shown. This analysis was made taking in consideration a number significant of regions (almost 5) over all the samples in order to obtain the adequate results to obtain a semi-quantitative amount of the Sm^{3+} quantities trapped during sol–gel synthesis. As it can be seen in Fig. 2, a region from sample with 0.5 wt% of Sm^{3+} prove that the sol–gel technique can give a homogenous distribution of Sm^{3+} and that the quantity of Sm^{3+} deposited was nearly to the theoretical calculated (see Table 2). In the case of the STEM-EELS (see Fig. 8) a pattern corresponding to Sm^{3+} [26] was obtained which confirm the oxidation state of the element.

3.2. Photocatalytic degradation of diuron

In Fig. 9 the photocatalytic degradation of diuron using solar light irradiation is shown. It is evident that photocatalytic degradation of diuron is obtained for activity tests carried out using sun radiation, which confirms the fact that most of them present Eg values which correspond to wavelengths higher than 400 nm (see

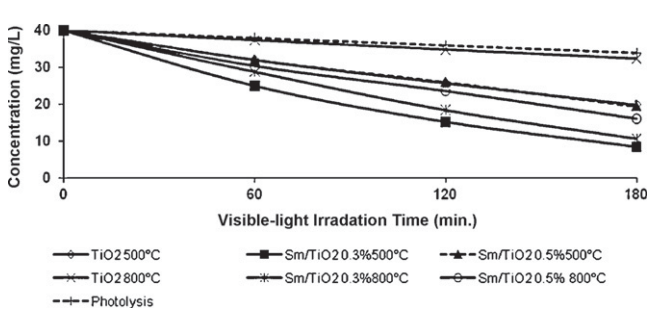

Fig. 9. Photocatalytic degradation of diuron using solar irradiation.

Fig. 7). Photocatalytic degradation of diuron did not reach 100% due to reaction conditions. Malato et al. reported the total degradation of diuron using the same amount of catalyst (500 mg/L), a lower concentration of diuron (22 ppm) and longer reaction times (200 min), however photocatalytic test was made using a parabolic solar concentrator [27].

By comparing the results in Fig. 9, it can be observed that, in the reactions with pure TiO_2 calcined at 500 °C and 800 °C, a large difference in the percentage of degradation exists. In the solid calcined at 500 °C, a 100% anatase phase is present and shows better results in photocatalytic process. The Eg of this material (3.02 eV) correspond to an absorption wavelength of 410 nm. This means that light with wavelength lower than 410 nm is required to promote the jump of electrons from valence band (VB) to the conduction band (CB) and generate photocatalytic phenomenon. When using this solar radiation the TiO_2 calcined at 500 °C is more photocatalytically active than the TiO_2 calcined at 800 °C, which only presents the rutile crystalline phase and a requirement of lower wavelength. Rutile phase is more stable, nevertheless it does not have photocatalytic effects because it does not promote the adsorption of the oxygen on its surface. We can observed that photocatalytic activity to TiO_2 calcined at 800 °C is practically the same showed by photolysis, in other hands the rutile activity is almost absent.

The samples doped with Sm^{3+} at 0.3 and 0.5 wt% and calcined at 500 °C developed large surface areas, the formation of anatase phase and Eg value in the range of 3.09–3.1 eV. For solids calcined at 800 °C, other physical characteristics were obtained such as: decrease in surface area, the formation of macropores, mixtures of crystalline phases (anatase–rutile) due to the generation of a surface Ti–O–M type bond in the TiO_2 which obstruct the complete formation of the rutile phase which keeps the anatase phase semistable at this temperature. Additionally, it presented a decrease in normal Eg values (2.8 eV) (see Table 2).

These modifications have an effect in the photocatalytic activity of the solids doped at 0.3 and 0.5 wt% and calcined at 500 °C. Furthermore, they show that with 0.3 wt% Sm^{3+}, a higher percentage of degradation is obtained than the observed for sample doped with 0.5 wt% Sm^{3+}. Photocatalyst doped with 0.3 wt% Sm^{3+} showed the highest activity with 80% of diuron degradation. The optimum percentage of dopant for Sm doped photocatalyst calcined at 500 °C and tested under solar radiation $\lambda > 400$ nm is then 0.3 wt%. Probably at higher Sm^{3+} content the Sm would be present at surface of particles and form clusters which do not favor the degradation processes that must be carried out at surface. For Sm^{3+} doping with 0.5 wt% degradation decreased to 42%, which is even lower than the activity shown by pure TiO_2 calcined at 500 °C, which confirms the fact that there exists a type of surface modification that is detrimental for photocatalytic activity.

Doping generates Ti–O–M bonds on the surface and substitutes the Ti–O–Ti bonds present on the TiO_2 surface which occurs when dopant metallic ions bond with superficial oxygen atoms and form tetrahedral oxides on the surface, which also are bonded to Ti atoms, thus forming vacancies of oxygen atoms and a non-equilibrium of charges or imbalance valences. The abundance of OH groups exhibited in the photocatalytic activity is due to the preparation method. When using an excess of water in the synthesis, these groups are preserved at the outside as well as the inside of doped TiO_2 as a result of the xerogel which was formed before thermal treating the samples. For this reason, it was important to extract the solvent (butanol) in order to break the Ti–OH bonds. The samples lost these OH groups at low rate only under high temperature treatment, producing defects on the surface, along with oxygen vacancies inducing an improvement in photocatalytic effects. This generates a disparity of charges to form more electron-hole pairs which generate radicals which oxidize and degrade diuron. In Fig. 10, plotting of $-\ln(C/C_0)$ versus time, which was used

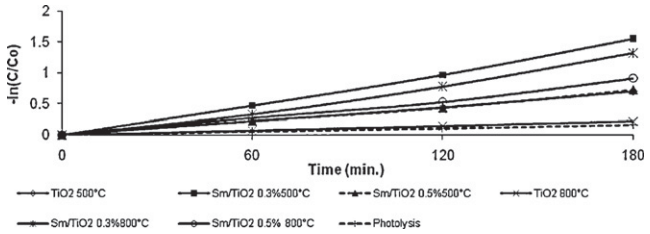

Fig. 10. Plotting $-\ln(C/C_0)$ versus time to calculate kinetic constants for the photocatalytic solar diuron degradation.

to calculate kinetic constants for the photocatalytic solar diuron degradation are shown. It can be observed that the reaction pursuit a pseudo first order behavior with a Langmuir–Hinshewood model. The kinetic constants calculated shown clearly the performance of the TiO_2 Sm^{3+} 0.3 wt% doped photocatalyst because the k value for this material is 0.0086 min^{-1}, the higher value of all the materials studied here. It is important to remark that the k value obtained for the material TiO_2 Sm^{3+} 0.3 wt% doped photocatalyst calcined at 800 °C was 0.0074 min^{-1} because considering that the same quantity of photocatalysts were used in all photocatalytic tests, and that the activity of rutile is practically zero, only 28% of the anatase of this material is active, thus, for photocatalyst treated at 800 °C the activity of anatase phase is higher than the observed for photocatalyst treated at 500 °C. Finally the activity observed for photocatalyst calcined at 800 °C results very attractive, considering the demand of photocatalytic materials for ceramic surfaces where firing treatments are required with temperatures around 800 °C.

4. Conclusions

Highly disperse Sm^{3+} on TiO_2 was effectively prepared by sol–gel method at concentrations of 0.3 and 0.5 wt%. The presence of these trivalent ions aided to reduce the anatase to rutile transformation during calcining treatments even at 800 °C. Besides a reduction on anatase transformation, photocatalyst showed a trend to reduce the band gap towards visible radiation region, which leaded to excellent results for photocatalytic degradation of diuron under sun radiation, so these materials can be the base for the development of industrial application of the photocatalysis on wastewater treatment.

References

[1] N.R. Serpone, F. Khairutdinov, Stud. Surf. Sci. Catal. 103 (1996) 191–203.
[2] K.J. Buechler, R.D. Noble, C.A. Koval, W.A. Jacoby, Ind. Eng. Chem. Res. 38 (1999) 1258–1263.
[3] P.S.M. Dunlop, J.A. Byrne, N. Manga, B.R. Eggis, J. Photochem. Photobiol. A 148 (2002) 355–363.
[4] A.-W. Xu, Y. Gao, H.-Q. Liu, J. Catal. 207 (2002) 151–157.
[5] M.G. Kang, H.-E. Han, K.-J. Kim, J. Photochem. Photobiol. A 125 (1999) 119–125.
[6] W. Zhou, Y.-H. Zheng, G.-H. Wu, 253, Appl. Surf. Sci. (2006) 1387–1392.
[7] C.-H. Liang, F.-B. Li, C.S. Liu, J.-L. Lu, X.-G. Wang, Dyes Pigments 76 (2008) 477–484.
[8] New Label Instruction for Diuron, *Pesticide News*, No. 25, September 2004.
[9] M. El Madani, C. Guillard, N. Pérol, J.M. Chovelon, M. El Azzouzi, A. Zrineh, J.M. Herrmann, Appl. Catal. B 65 (2006) 70–76.
[10] S. Malato, J. Blanco, A. Vidal, D. Alarcón, M. Maldonado, J. Cáceres, G. Wolfgang, Solar Energy 75 (2003) 329–336.
[11] M. Canle-Lopez, M.I. Fernandez, S. Rodríguez, J.A. Santaballa, S. Steenken, ChemPhysChem 6 (10) (2005) 2064–2074.
[12] M.V. Shankar, S. Nélieu, L. Kerhoas, J. Einhorn, Chemosphere 66 (4) (2007) 767–774.
[13] S. Malato, J. Caceres, A.R. Fernández-Alba, L. Piedra, M.D. Hernand, A. Aguera, J. Vidal, Environ. Sci. Technol. 37 (2004) 2516–2524.
[14] M.M. Higarashi, W.F. Jardim, Catal. Today 71 (2002) 201–207.
[15] K.M. Parida, S. Nruparaj, J. Mol. Catal. A 287 (2008) 151–158.
[16] J.A. Eastman, J. Appl. Phys. 75 (1993) 770–779.
[17] JCPDS PDF-2 pattern 21-1272.
[18] JCPDS PDF-2 pattern 21-1276.
[19] P.T. Moseley, Sens. Actuators B 6 (1992) 149–156.

[20] V. Guidi, M.C. Carotta, M. Ferroni, G. Martinelli, M. Sacerdoti, J. Phys. Chem. B 107 (2003) 120–124.
[21] H. Zhang, J. Banfield, J. Mater. Res. 15 (2000) 437–448.
[22] M.S.P. Francisco, V.R. Mastelaro, Chem. Mater. 14 (2002) 2514–2518.
[23] J. Lin, J.C. Yu, J. Photochem. Photobiol. A 116 (1998) 63–67.
[24] C. Anderson, A.L. Bard, J. Phys. Chem. B 101 (1997) 2611–2616.
[25] R. Silveyra, L. De La Torre Sáenz, W. Antúnez Flores, V. Collins Martínez, A. Aguilar Elguézabal, Catal. Today 107–108 (2005) 602–605.
[26] http://www.cemes.fr/∼eelsdb/index.php?page=search.php&searchelt=Sm.
[27] S. Malato, J. Cáceres, A.R. Fernández-Alba, L. Piedra, M.D. Hernando, A. Agüera, J. Vial, J. Environ. Sci. Technol. 37 (2003) 2516–2524.